IEEE Access
Multidisciplinary ⋮ Rapid Review ⋮ Open Access Journal

Received 27 January 2025, accepted 24 March 2025, date of publication 27 March 2025, date of current version 7 April 2025.

Digital Object Identifier 10.1109/ACCESS.2025.3555388

RESEARCH ARTICLE

Auto-Induced Downlink Radiofrequency Electromagnetic Field Exposure at 3.5 GHz With Focusing Near the Head

HANNE HERSSENS[1] AND ARNO THIELENS[2], (Senior Member, IEEE)

[1]Department of Information Technology, Ghent University, 9000 Ghent, Belgium
[2]Photonics Initiative, Advanced Science and Research Center, Graduate Center of the City University of New York, New York, NY 10031, USA

Corresponding author: Hanne Herssens (hanne.herssens@ugent.be)

This work was supported by the Exposure to Electromagnetic Fields and Planetary Health (ETAIN) Project, funded by European Union's Horizon Europe Research and Innovation Funding Program under Grant 101057216.

ABSTRACT The auto-induced downlink exposure at 3.5 GHz is evaluated in networks where the power density is focused at the user equipment (UE), leading to a highly localized exposure. To achieve this focusing, various precoding techniques can be applied. Two of these are compared using Finite-Difference Time-Domain simulations. For each technique, three different exposure scenarios are considered: UE located next to the ear (phone call), UE located in front of the eyes, and the nose (video call). The exposure is evaluated in terms of the localized specific absorption rate using a female and a male phantom. We find that the exposure highly depends on the location of the UE and precoding technique. According to the International Commission on Non-Ionizing Radiation protection (ICNIRP)'s guidelines, this exposure should be normalized to the maximum incident power density. In this work, we suggest normalization strategies of this highly focused exposure and compare these. We show that the choice of normalization can create a situation where the ICNIRP basic restrictions can be exceeded while complying with the reference levels. This is important because compliance with the reference levels should ideally ensure compliance with the basic restrictions.

INDEX TERMS 5G, FDTD, focused exposure, RF-EMF exposure.

I. INTRODUCTION

The 5th generation of telecommunication (5G) is currently being rolled out worldwide. This raises some public concern about the potential health effects of radiofrequency electromagnetic fields (RF-EMFs) emitted by these technologies. Therefore, it is important to assess RF-EMF exposure in such networks. Guidelines that limit RF-EMF exposure are provided by the International Commission on Non-Ionizing Radiation Protection (ICNIRP) [1]. In the frequency range of interest here, ICNIRP works with two different exposure quantities: reference levels, i.e., incident field strengths and power densities, and basic restrictions, i.e., specific absorption rates (SAR) [1]. Compliance with the former can be determined in situ, i.e., in actual exposure scenarios in the field by performing RF-EMF measurements, while the latter can only be determined in the lab or in silico. It is these absorption quantities that are related to potential health effects in the human body, such as dielectric heating. In general, the goal of having reference levels is to ensure compliance with the basic restrictions. If one can show compliance with the reference levels, it should be the case that compliance with the basic restrictions follows automatically. This has been heavily investigated and shown for legacy technologies (up to 4G) [1]. As an example, a simulation study conducted in [2] shows that for an adult exposed to an incident plane wave at frequencies below 6 GHz under various incidence angles and polarizations, the guidelines are never exceeded when the incident power density is set to the reference level. However, it is not yet

The associate editor coordinating the review of this manuscript and approving it for publication was Amjad Ali.

© 2025 The Authors. This work is licensed under a Creative Commons Attribution 4.0 License.
For more information, see https://creativecommons.org/licenses/by/4.0/

established whether this also holds for the new techniques used in 5G new radio (NR) networks. One of the goals of this paper is to investigate this.

The base stations (BS) in 5G networks are enabled with Multiple-Input-Multiple-Output (MIMO) technology [3]. These BSs consist of an antenna array with a large number of elements. The BS can use the knowledge of channels that are available to configure these elements in such a way that the EMFs are targeted at users (constructive interference) and potentially reduced at non-users (destructive interference). This is known as precoding. In line-of-sight (LOS) conditions, a beam will be formed towards the user equipment (UE). In non-line-of-sight (NLOS) conditions, an EMF hotspot will be formed at the UE. This precoding leads to a higher signal-to-noise ratio (SNR). This is a significant difference compared with legacy technologies (2G-4G), in which data transmission occurs over fixed beams. Therefore, in these technologies, the downlink (DL) exposure did not depend on one's usage and this type of exposure could be assessed as is done in [4], i.e., by assuming that DL exposure consists either of a set of uncorrelated plane waves or correlated plane waves whose distribution depends on fading properties of the environment. In 5G, the DL exposure highly depends on being a user or not. Additionally, the exposure will depend on the location of the UE. In literature, this type of exposure is called auto-induced DL (a-DL) exposure [5]. The focus of this paper is the development of a method for quantifying this type of exposure.

Different methods exist to take this precoding into account when assessing the RF-EMF exposure in 5G networks. One way to do this is theoretically. In [6], the realistic maximum exposure for an antenna array using precoding is determined using analytical expressions. The authors of [7] use the 3D spatial channel model developed by 3GPP to stochastically assess the exposure. The antenna arrays that enable this precoding can also be modeled using full-wave simulations [8]. However, it is often difficult to include both the antenna and the phantom in a single FDTD simulation, and therefore different hybrid methods are proposed in literature. In [9], a hybrid spherical near-field transformation with FDTD is proposed. In [10], [11], and [12], a hybrid ray-tracing/FDTD method is used, in which the ray-tracing is used to model the environment and the FDTD method to assess the exposure due to incident EMFs resulting from the ray-tracing. In these environments, the BS antenna arrays are located in a certain direction relative to the user. In some situations, this leads to the UE being shadowed, i.e., the human body blocks the signals from the BS to the UE [12], [13], [14]. In this work, we want to make an abstraction of the potential environment and therefore we will not model a particular environment, but we will assume that the EMFs can be incident from anywhere, i.e., there will be no dominant direction of arrival which could lead to the UE being shadowed by the human body. Instead, since EMFs can be incident from all possible directions, there always exist unobstructed paths. Here we are considering an idealized situation in which all channels or equivalently all angles of incidence are available for the system for achieving focusing and consequently a higher SNR. This approach was already used in [15]. In [15], the UE was located next to the ear emulating a phone call. The highest EMFs were found near the UE, i.e., near the ear. As a result, the highest exposure was found when the UE was located inside the ear, which would be the case with implants. This can be explained by the fact that even with plane wave exposure, at 3.5 GHz, the peak SAR is found in body parts with small dimensions and high curvature like the ear [2]. In this work, we will also look at other UE locations near the head. For this, we will work at 3.5 GHz. We have chosen this frequency, because this is the center frequency of the 3.3 to 3.8 GHz 5G-NR frequency band (n78) which is currently being rolled out in the EU and in which this precoding could be used. None of the discussed related works in literature look at how the localized exposure depends exactly on the location of the UE. The goal of this work is to determine the a-DL exposure in terms of the localized absorption for different UE locations near the head. The main contributions of this paper are:

- Multiple locations of the UE are considered and compared, that is, near the ear and in front of the eyes.
- The localized absorption is determined as a function of distance between the UE and the user using numerical simulations.
- Both a female and male phantom are used.
- Two different precoding techniques are considered and the result on the exposure is compared.
- Different normalization strategies of the exposure quantities related to the reference levels and basic restrictions, respectively are discussed, in order to study compliance with the ICNIRP guidelines.

Table 1 summarizes the related literature and how this work relates to and differentiates itself from it.

The outline is as follows. Section II describes the methods that were used to determine the a-DL exposure. Section III provides the results. The focusing effect is quantified, the exposure for different UE locations is compared, and the different normalization strategies are applied and compared with the international guidelines. Section IV contains the conclusion.

II. MATERIALS AND METHODS

The chosen methodology consists of two big parts. In the first part, plane wave simulations will be performed. The results of these simulations are the input of the second part. In the second part, precoding will be applied and the focused exposure is determined. Fig. 1 shows a scheme of the methodology. The different parts will be explained in more detail in the following sections.

A. FDTD SIMULATIONS

Numerical simulations are performed using the Finite-Difference Time-Domain (FDTD) method in Sim4Life (ZMT, Zürich, Switzerland). It is assumed that the user is

TABLE 1. Overview of related works.

Work	Goal	Methodology	Contribution
This work	Determine the a-DL exposure for different locations of the UE near the head	FDTD	The exposure following precoding is assessed for UE located next to the ear and in front of the eyes. The localized absorption is determined as a function of distance between the UE and user. The results using a female and male phantom are compared. Different normalization strategies in regards to the incident power density are proposed and compared.
[6]	Determine realistic exposure due MIMO networks	Statistical approach	A theoretical model for the time-averaged realistic maximum power levels for 5G BS is presented.
[7]	Determine realistic exposure due MIMO networks	Statistical approach	The compliance boundary is determined for realistic deployment scenarios.
[8]	Determine exposure due 5G access point	FDTD	The localized exposure was determined in a 5G indoor scenario for different antenna positions towards the human model.
[9]	Determine exposure due 5G antenna array	Hybrid SNFT/FDTD	The exposure and temperature rise due to four different antenna arrays is determined for different configurations.
[10]	Determine realistic exposure due MIMO networks	Hybrid RT/FDTD	The localized exposure following EGT precoding at the BS is determined.
[11]	Determine realistic exposure due MIMO networks	Hybrid RT/FDTD	The localized exposure following MRT precoding at the BS and accounting for the effect of near-field coupling between antenna and user is determined.
[12]	Determine realistic exposure due collocated and distributed MIMO networks	Hybrid RT/FDTD	The localized exposure following precoding at the BS in collocated and distributed MIMO networks is compared.
[15]	Determine a-DL exposure when the UE is located next to the head.	FDTD	The localized exposure following EGT and MRT precoding is determined for different distances between UE and ear.

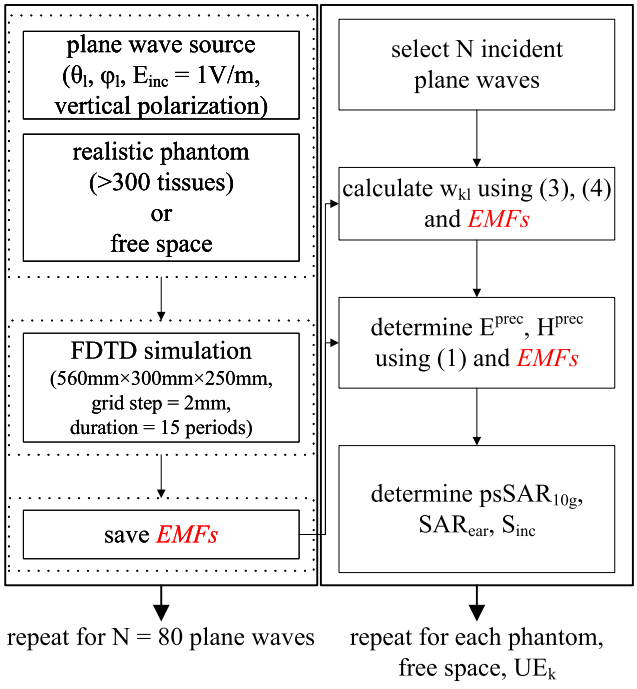


FIGURE 1. Scheme of the chosen methodology consisting of plane wave simulations and precoding and how these intersect.

situated in the far-field of the BS, i.e., $R > 2D^2/\lambda$, with R the distance between the user and BS, D the size of the antenna and $\lambda = 86\,\text{mm}$ the wavelength at 3.5 GHz. Therefore, the incident EMFs can be modeled as plane waves [16]. Additionally, we assume that the fields can be incident from all possible directions, i.e., from any ϕ and θ defined by the coordinate system shown in the top right in Fig. 2. The origin of the coordinate system is coincident with the center of the phantom's head and the FDTD domain, which is limited to the blue box shown in the top right of Fig. 2. The FDTD domain (560 mm × 300 mm × 250 mm) only includes the head of the phantom for both Duke and Ella to reduce the simulation size (Fig. 2). This is done by cutting the Ella and Duke phantom at 1405 mm and 1567 mm, respectively, starting from the bottom in the z-direction. The domain is extended in the x-direction compared with [15] such that the UE can be located up to 200 mm from the eyes, which corresponds with realistic usage positions. The purpose of this work is not to evaluate RF-EMF exposure for current 5G NR networks. In contrast, this work investigates what the RF-EMF exposure would be when a MIMO system would be deployed in the 3.5 GHz frequency band in order to predict future exposures, similar to [10]. We want to investigate what could be achieved in terms of focusing and consequently exposure when the incident fields are incident from anywhere. In total, 80 simulations are performed with the wave vectors of the plane waves distributed uniformly over the unit sphere [11]. This is equivalent to a virtual, large antenna system formed with the UE at its center. The plane waves are vertically polarized (E_θ-polarization) and the duration of each simulation is set to 15 periods leading to a steady state. Two different heterogeneous phantoms are used in this paper, i.e., the ViP Duke and Ella phantoms [17]. These phantoms consist of more than 300 tissues for which the dielectric parameters are found in [18]. A grid step of 2 mm in each direction is chosen. Different locations of the UE are investigated (white dots in Fig. 2), i.e., next to the left ear, in front of the eyes, and in front of the nose (II-C). The UE is considered a virtual device with vertical polarization (E_z-polarization).

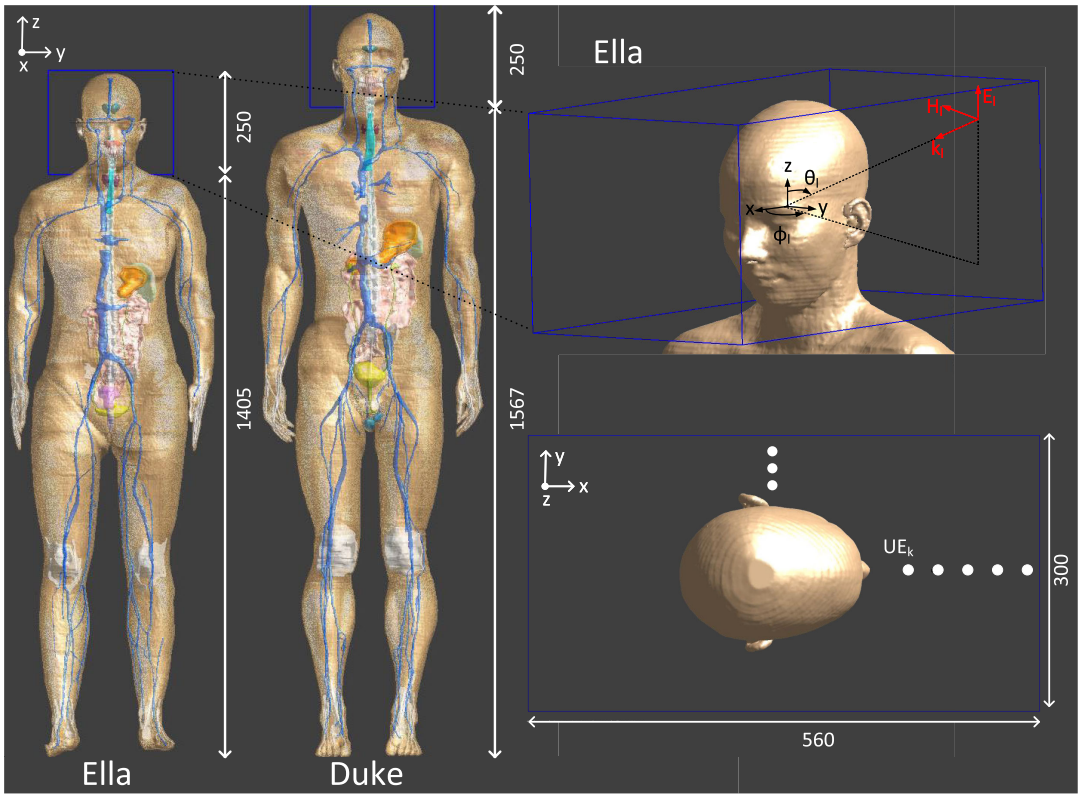


FIGURE 2. Simulation setup. The FDTD domain (560 mm × 300 mm × 250 mm) is indicated by the blue box. Left: whole-body phantoms. Top right: The Ella phantom with incident plane wave *l* in red. Bottom right: Top view of the Ella phantom with the possible locations of UE *k*, i.e., next to ear and in front of eyes and nose, shown by the white dots. All dimensions are given in mm.

B. PRECODING TECHNIQUES

Two different precoding techniques are applied to ensure that the EMFs will interfere constructively at the UE location. If these EMFs were combined without any precoding, the random real and imaginary components would combine incoherently. To avoid this, precoding will ensure that the phases of the individual EMFs will be coherent at the UE by multiplying the different EMFs by a complex weight, leading to a focusing of the EMFs [19]. The electric field focused at UE k is written as

$$\mathbf{E}_k^{prec}(\mathbf{r}) = \sum_{l=0}^{N-1} \alpha_k w_{kl} \mathbf{E}_l(\mathbf{r}) \tag{1}$$

with N the number of plane waves, α_k a normalization constant, w_{kl} the precoding weight, and $\mathbf{E}_l(\mathbf{r})$ the electric field obtained with plane wave l at position $\mathbf{r}$. The precoding is normalized with normalization constant:

$$\alpha_k = \frac{1}{\sqrt{\sum_{l=0}^{N-1} w_{kl}^2}}. \tag{2}$$

The precoded magnetic field $\mathbf{H}_k^{prec}(\mathbf{r})$ can be obtained by substituting $\mathbf{E}$ with $\mathbf{H}$ in (1).

Two different precoding techniques are applied. The first precoding technique is equal gain transmission (EGT). With this technique, the BS antennas will configure their phases to obtain coherent phases at the UE [10], [19]. Some of the BS antennas can result in low EMFs at the UE. These will be equally weighted with this technique, resulting in low EMFs after precoding. This issue is resolved with the second technique. The second precoding technique is maximum ratio transmission (MRT). With this technique, the BS antennas will configure their amplitudes and their phases, resulting in a higher SNR at the UE [11], [12], [19], [20]. The precoding weights, when focusing at UE k, can be written as

$$w_{kl}^{EGT} = \exp\left(-j \cdot arg(E_{z,kl})\right) \tag{3}$$
$$w_{kl}^{MRT} = E_{z,kl}^{*}, \tag{4}$$

where $*$ indicates the complex conjugate and $E_{z,kl}$ the z-component of the electric field at UE k obtained with incident plane wave l. The z-component is used for the precoding, since the UE is vertically polarized.

C. CONFIGURATIONS

Three different configurations are considered in terms of the UE location corresponding to real-life situations. The exposure is then assessed as a function of the distance between the phantom and the focus point (UE location), see Fig. 2.

1) FOCUSING AT THE EAR

In the first configuration, the UE is located next to the left ear. The x- and z-coordinates are chosen at approximately the location in which a phone would be held when making a phone call and are held constant for the considered focus points, while the y-coordinate is varied. The smallest y-coordinate corresponds to a distance of −6 mm between the ear and the UE, i.e., the focus point is found in the ear, corresponding to an in-ear device with 5G NR capabilities such as smart hearing or earbuds.

2) FOCUSING AT THE EYES

In the second configuration, we consider the situation when a video call is made, i.e., the UE is found in front of the eyes. Here, the x-coordinate is varied, while the y- and z-coordinates of the focus point are kept constant. The smallest y-coordinate corresponds with a distance of 0 mm between the eyes and the UE, which would be the case when wearing a smart contact lens.

3) FOCUSING AT THE NOSE

Additionally, we look at the case where the UE is positioned at the height of the nose, i.e., the same x- and y-coordinates of the UE location as the above configuration is considered but the UE is placed at a lower height ($z_{nose} < z_{eyes}$). This case is considered, since we know that EMFs concentrate around high curvatures. Therefore, this can be considered a worst-case scenario when looking at your phone.

D. POWER DENSITY FOCUSING

The focusing effect is quantified for the UE located 30 mm from the ear of the Ella phantom. Since the phantom is approximately symmetric with respect to the mid-saggital plane (xz-plane), the ratio of the power density at the UE ($||Re[\mathbf{S}(\mathbf{r}_{UE})]||$) and at the symmetric location of the UE with respect to the xz-plane ($||Re[\mathbf{S}(\mathbf{r}_{symm})]||$) is determined:

$$S_{ratio}(dB) = 10 \cdot log_{10}\left(\frac{||Re[\mathbf{S}(\mathbf{r}_{UE})]||}{||Re[\mathbf{S}(\mathbf{r}_{symm})]||}\right). \quad (5)$$

This is done for 100 samples when taking N random incident plane waves.

E. EXPOSURE QUANTITIES

The EMFs will be highly focused at the UE. Therefore, the a-DL exposure will be highly localized. For this reason, the peak-spatial SAR averaged over a 10 g cube ($\mathrm{psSAR_{10g}}$) is considered. This exposure quantity is standardized by the ICNIRP as the local basic restriction at 3.5 GHz. Basic restrictions are closely related to the RF-EMF induced health effects inside the exposed body, but cannot be easily measured. The ICNIRP defines two tissue types for setting local exposure limits. These tissue types each have a different temperature rise threshold and therefore another associated basic restriction limit. The tissue types that are considered in this study are the pinna (ear), eye, and the rest of the head. The pinna and the cornea, anterior chamber and iris of the eye, belong to Type-1, while the rest of the head and eye belongs to Type-2. Type-1 and Type-2 tissues allow a temperature rise of 5 °C and 2 °C, respectively. To make the analysis easier, ICNIRP has reduced these different tissues to only two regions, i.e., the head and torso region (Type-1 and Type-2 tissues) and the limbs region (only Type-1 tissues). Note that in the IEEE-C95.1 standard, the pinna is treated separately from the head [21]. In this work the ICNIRP guidelines are followed and we will not treat the pinna separately. The limit of the basic restriction is set to 2 W/kg for the general public [1].

Additionally, the organ-specific averaged SAR in the left ear ($\mathrm{SAR_{ear}}$) is considered, since a high exposure is often found in the ear due to its high curvature [2], [11] and the mass is approximately 10 g (8.6 g and 10.6 g for Ella and Duke, respectively). The organ-specific averaged SAR provides information about the absorption in a certain tissue, in this case the ear, while the 10 g cube considered in the $\mathrm{psSAR_{10g}}$ does not have to belong to one specific tissue. In the case of a 10 g cube near/at the ear, the cube will not only contain connected tissue, but will also contain some air. Furthermore, in the first configuration (II-C) the UE is placed next to the left ear, which makes the SAR averaged over the ear a suitable quantity.

The reference level at 3.5 GHz is the incident power density ($\mathrm{S_{inc}}$). Reference levels are a proxy for the basic restrictions, but have the advantage that they can more easily be measured. The maximum allowed value set by ICNIRP is 40 $\mathrm{W/m^2}$ for local exposure [1]. We define the normalized exposure quantity β as the ratio between the basic restriction and the reference level [11]:

$$\beta\ [\mathrm{m^2/kg}] = \frac{\mathrm{psSAR_{10g}\ [W/kg]}}{\mathrm{S_{inc}}(\mathbf{r})\ [\mathrm{W/m^2}]} \quad (6)$$

$$\mathrm{S_{inc}}(\mathbf{r})\ [\mathrm{W/m^2}] = \frac{1}{V}\int_V \frac{||Re(\mathbf{E}\times\mathbf{H}^*)||}{2} dV. \quad (7)$$

With single plane wave exposure, the incident power density is constant in space. This is no longer the case with focused exposure, since the power density can rapidly change near the focus point (Fig. 5). Therefore, we define the sampling location $\mathbf{r}$ (7) to keep track of where the power density $\mathrm{S_{inc}}$ is sampled, where $\mathrm{S_{inc}}(\mathbf{r})$ indicates the power density at point $\mathbf{r}$. Different sampling locations will lead to different normalized exposure quantities. The definition of the incident power density used in the ICNIRP guidelines is the peak spatial value projected over the whole-body space. We know that an EMF hotspot will be formed at the UE with an expected hotspot size of 51 mm at 3.5 GHz [10]. Therefore, in this paper, three other normalization strategies are suggested that involve a different integration using (7) which differ in the sampling location and volume, which takes this focusing more into account compared to the ICNIRP definition. The constant β gives us insight into whether the ICNIRP basic restrictions can be exceeded while complying with the ICNIRP reference levels at 3.5 GHz using these different

definitions of incident power density. When following the limits set by ICNIRP, a $\beta_{\text{ICNIRP}} = 0.05\,\text{m}^2/\text{kg}$ is found. Any exposure situation with $\beta \leq 0.05\,\text{m}^2/\text{kg}$ corresponds to a situation in which the basic restriction is not exceeded when one adheres to the reference level, while $\beta > 0.05\,\text{m}^2/\text{kg}$ indicates that the basic restriction can be exceeded while adhering to the reference level. The latter situation is a situation that one wants to avoid from a compliance point of view.

We analyze coherent exposure at a single harmonic frequency, that is, 3.5 GHz. A MIMO system will use different frequency slots. In each of these slots, the same techniques could be used. SAR values in the different frequency bands used by such a system should be determined prior to determining the psSAR_{10g}.

F. NORMALIZATION STRATEGIES

In this section, the different normalization strategies with their rationale are explained based on different definitions of S_{inc}.These different definitions are illustrated in Fig. 3. Note that only a cross-section of the domain is shown, but that the averaging occurs over the whole three-dimensional domain.

1) NORMALIZATION TO MAXIMUM INCIDENT POWER DENSITY IN FREE SPACE

In the first normalization strategy, the considered exposure quantity is normalized to the maximum incident power density found in the domain when no phantom is present ($S_{inc,max}$), see white cross in Fig. 3, top. This leads to the normalized exposure quantity β_{max}. This type of normalization is denoted as hot-spot normalization in [11] and is the normalization following the ICNIRP guidelines [1].

2) NORMALIZATION TO AVERAGE INCIDENT POWER DENSITY IN FREE SPACE

In the second normalization strategy, the considered exposure quantity is normalized to the average incident power density in the domain when no phantom is present ($S_{inc,avg}$). This leads to the normalized exposure quantity β_{avg}. For this type of normalization, the power density obtained with the precoded plane waves in (1), averaged over the domain when no user is present, is used. In this study, it will be averaged over a volume of 560 mm × 300 mm × 250 mm (Fig. 3, top). The normalized exposure β_{avg} will depend on the size of the computational domain. A hotspot will be present in the domain and will be of the order 51 mm in free space [10]. This means that a larger domain will introduce lower power density values away from this hotspot, thus a larger domain will lead to a lower $S_{inc,avg}$ and therefore to a higher β_{avg}. Note that this normalization strategy is not realistic to apply in practice, but it provides valuable insights in how the fields behave around a focus point.

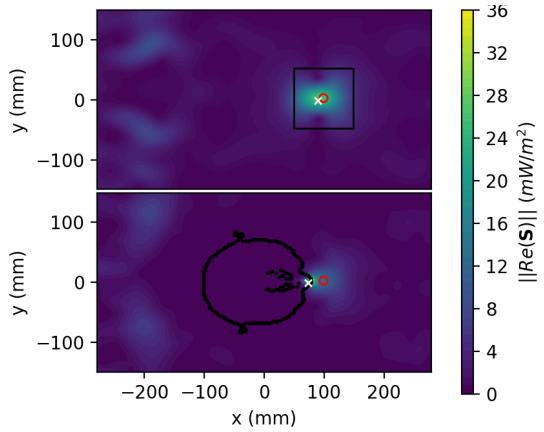


FIGURE 3. Illustration of the different definitions of S_{inc} (reference level). The power density focused at the UE located in front of the eyes in the xy-plane ($z = z_{focus}$) for the Ella phantom using MRT precoding. The precoding weights are normalized according to (2). The power density without (top, normalization 2) and with (bottom) phantom is shown. White cross: maximum power density (top, normalization 1). Red circle: focus point (bottom, normalization 3). Black square: averaging volume V_{avg} = 100 mm × 100 mm × 100 mm (top, normalization 4).

3) NORMALIZATION TO INCIDENT POWER DENSITY AT FOCUS POINT

In the third normalization strategy, the considered exposure quantity is normalized to the incident power density found at the UE location ($S_{inc,focus}$) when the phantom is present, see red circle in Fig. 3, bottom. This leads to the normalized exposure quantity β_{focus}. This scales directly with the signal strength needed by the UE to operate (S_{UE}), i.e., $\text{psSAR}_{10g} = \beta_{focus} * S_{UE}$. This strategy is proposed from a practical standpoint. It has the advantage that if one knows what the needed power density is for the device to operate, the exposure automatically follows.

4) NORMALIZATION TO AVERAGE INCIDENT POWER DENSITY AROUND FOCUS IN FREE SPACE

In the fourth normalization strategy, the considered exposure quantity is normalized to the average incident power density around focus when no phantom is present ($S_{inc,V_{avg}}$), that is, the power density averaged over a certain volume (V_{avg}) centered around the focus point (UE), see black square in Fig. 3, top. This leads to the normalized exposure quantity $\beta_{V_{avg}}$. The previous normalization strategies are extreme cases: on one end of the spectrum, we looked at averaging the power density over the entire computational domain, or on the other extreme, we look at the power density at one individual point. In this strategy, we try to find a middle ground. Since we know that the a-DL power density is highly focused around the UE. This type of normalization would take the size of the hotspot into account, which we expect to be around 51 mm at 3.5 GHz [10]. The side length of V_{avg} is varied from 0 cm (focus point) to 10 cm leading to volumes from 0 cm^3 (focus point) to 1000 cm^3.

III. RESULTS AND DISCUSSION

A. POWER DENSITY FOCUSING

Fig. 4a shows the cumulative distribution function (cdf) of S_{ratio} for different numbers of incident plane waves N. S_{ratio} quantifies the focusing effect. Its median values are 4 dB, 6 dB and 7 dB for 10, 50, and 80 plane waves, respectively, using EGT precoding. Using MRT precoding, the median values are 12 dB, 17 dB, and 18 dB for 10, 50, and 80 plane waves, respectively. More plane waves will lead to a higher ratio, i.e., stronger focusing. The focus point (UE) will be shadowed by the human body for a part of the incident plane waves [12], [13]. These particular plane waves will contribute less at the focus point with MRT precoding, while the contribution with EGT precoding will be equal. As a result, a stronger focus (S_{ratio}) is found by using MRT precoding. If no precoding is present, $S_{ratio} = 0$ dB on average due to the symmetry, because the random real and imaginary components will add incoherently. Fig. 4b shows the 50th and 95th percentiles as a function of the number of incident plane waves. Increasing the number of plane waves from 50 to 80 does not lead to a big increase in the focusing effect, that is, the median value p_{50} increases only 0.5 dB. Therefore, in the following sections, $N = 80$ is chosen for the case where each plane wave occurs only once. This leads to $S_{ratio} = 7$ dB and 21 dB using EGT and MRT precoding, respectively, which is comparable to the median values obtained when using 80 random plane waves as shown in Fig. 4.

Fig. 5 plots the focused power density for the Ella and Duke phantom using the MRT precoding. As mentioned in the previous paragraph, the precoding occurs using all 80 plane waves with the wave vectors distributed uniformly over the unit sphere. The UE location is indicated by the red circle and is found at a distance 25 mm next to the left ear in Fig. 5a and 100 mm in front of the eyes in Fig. 5b representing realistic use cases. A high power density is found near the UE in both cases. This is the result of the precoding which ensures that the individual EMFs combine coherently at the UE, that is, the phases are 0 at this location. When focusing next to the ear, the maximum power density is found at the ear instead of the intended focus point. High curvatures, such as the ears or nose, are known to lead to elevated EMFs [2]. This can also be seen when focusing in front of the eyes, where a high power density is found near the nose. In this case, a high symmetry in the power density is seen with respect to the xz-plane. This is expected because the phantom is (approximately) symmetric with respect to the xz-plane, the focus point lies at approximately $y = 0$ mm and the plane waves are distributed uniformly over the unit sphere. The focusing effect can also be quantified by looking at the hotspot size, which gives an indication of how centered the obtained fields are at the UE. The hotspot size is quantified by the full width at half maximum along the x- ($\mathrm{FWHM_x}$) and y-direction ($\mathrm{FWHM_y}$) when $z = z_{focus}$ for the case in Fig. 5b. The $\mathrm{FWHM_x}$ is 56 mm and 58 mm when using the Duke and Ella phantom, respectively. The $\mathrm{FWHM_y}$ is 44 mm when using the Duke and Ella phantom, respectively. The longer FWHM along the x-direction is expected since the focus point lies on the phantom's symmetry plane, i.e. the xz-plane.

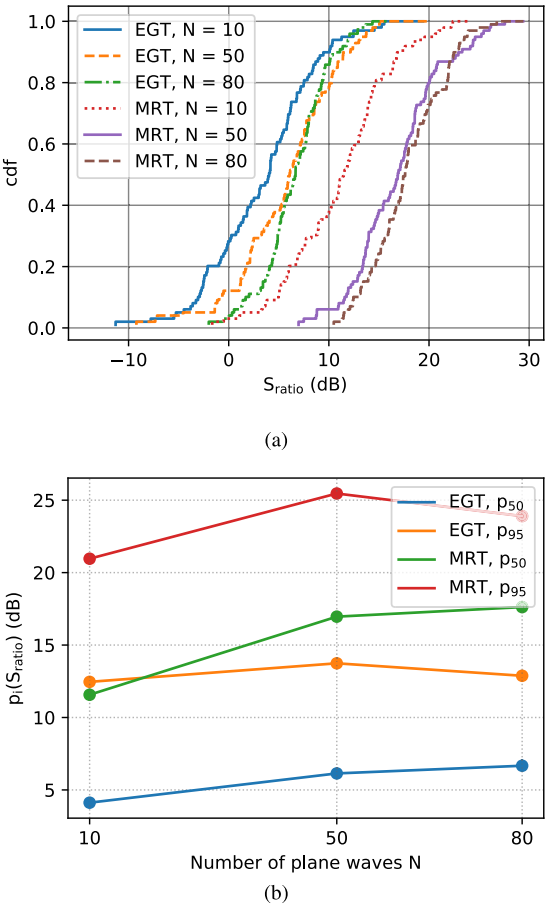


FIGURE 4. (a) Cumulative distribution function (cdf) of S_{ratio} for a different number of plane wave sources N. (b) The 50th and 95th percentiles of S_{ratio} as a function of number of incident plane waves.

B. EXPOSURE ASSESSMENT

1) FOCUSING AT THE EAR

Fig. 5a shows that a high power density is found near the ear when the focus point is located next to it. This illustrates that $\mathrm{SAR_{ear}}$ is a suitable exposure quantity for this exposure scenario. $\mathrm{SAR_{ear}}$ (orange and blue curves) as a function of distance for the Ella and Duke phantoms is plotted in Fig. 6. The behavior of $\mathrm{SAR_{ear}}$ for both phantoms is similar for both precoding techniques. In general, $\mathrm{SAR_{ear}}$ decreases as a function of distance. This is a result of the precoding, since this ensures that the high fields are concentrated around the focus point. Using MRT, $\mathrm{SAR_{ear}}$ starts increasing again from approximately 60 mm. The simulations were only performed up to a distance of 75 mm (computational domain), but it is expected that $\mathrm{SAR_{ear}}$ will increase up to approximately a distance of $\lambda = 86$ mm. Using EGT, a local maximum is also found at a distance of approximately $\lambda/2$ for the same reason.

The $\mathrm{psSAR_{10g}}$ (green and red curves) as a function of distance is also plotted in Fig. 6, which is the ICNIRP basic

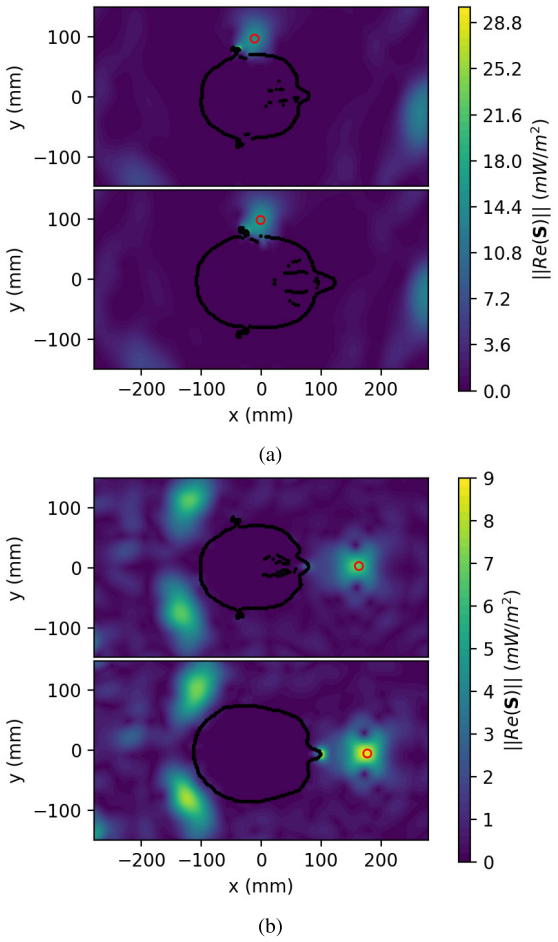


FIGURE 5. The power density focused at the UE (red circle) located (a) next to the ear and (b) in front of the eyes in the xy-plane ($z = z_{focus}$) for the Ella (top) and Duke (bottom) phantom using MRT precoding. The precoding weights are normalized according to (2).

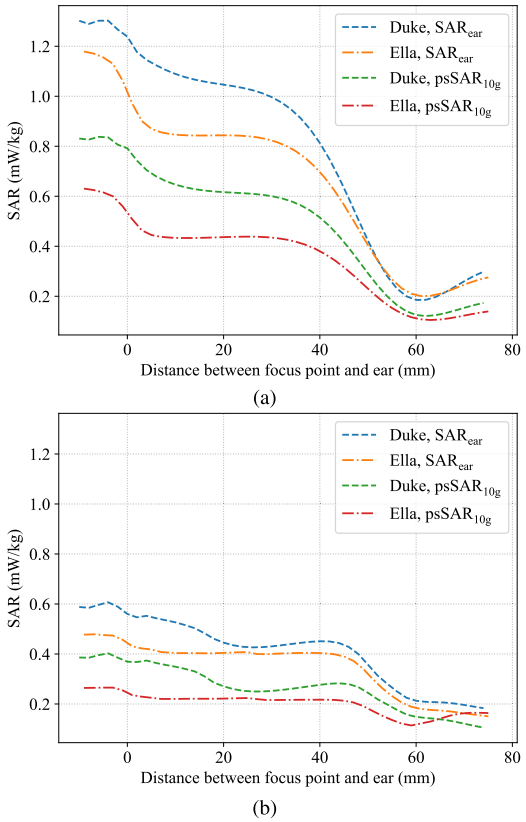


FIGURE 6. Comparison of SAR_{ear} and $psSAR_{10g}$ (basic restriction) as a function of distance between the focus point and the ear of the Duke and Ella phantom. The UE is located next to the ear. (a) MRT. (b) EGT. The precoding weights are normalized according to (2).

restriction. This exposure quantity follows the same behavior as SAR_{ear}, but has lower values. These lower values are the result of the fact that the 10 g cube used to determine $psSAR_{10g}$ will contain some air due to the location and high curvatures of the ear. As an example, for the Ella phantom when focusing at a distance of 25 mm (Fig. 5a), the $psSAR_{10g}$ is 0.44 mW/kg compared to a SAR_{ear} value of 0.84 mW/kg for a power density of 0.015 W/m^2 at the UE. The peak is often found in the ear when focusing next to it. This is in line with [10] and [11]. Only for the Ella phantom, using EGT, the peak is not found in the ear for distances $>$ 59 mm. As a result, in Fig. 6b, $psSAR_{10g}$ starts increasing from 59 mm, while SAR_{ear} does not for the Ella phantom, indicating that $psSAR_{10g}$ is not located at the same location as SAR_{ear}. The $psSAR_{10g}$ is situated in the range 0.1-0.4 mW/kg and 0.1-0.8 mW/kg using EGT and MRT, respectively. The authors of [10] found similar values for a similar exposure situation when EGT is applied and the same incident power density, i.e., $psSAR_{10g}$ values in the range 0.05-0.4 mW/kg (NLOS conditions) and 0.4-1.5 mW/kg (LOS conditions).

2) FOCUSING AT THE EYES

Fig. 7 plots the $psSAR_{10g}$ when focusing in front of the eyes using MRT precoding. Two different heights of the focus point are compared, i.e., a focus point at the height of the eyes (z_{eyes}) and at the height of the nose (z_{nose}). The last situation is considered to represent a worst-case scenario, since it is known that the curvature of the nose will lead to high EMFs [2]. The red-shaded area indicates the border of the eyes and nose. Again, similar results are obtained for the Ella (Fig. 7a) and Duke (Fig. 7b) phantoms. Higher values are obtained for $z_{focus} = z_{nose}$, especially when the focus point is located near or in the nose (red-shaded area) due to its shape, which leads to high EMFs. Both phantoms show a maximum in this area, after which the $psSAR_{10g}$ decreases up to a distance of approximately 150 mm with a small peak at 90 mm. For distances larger than this value, the peak SAR is found in the ear, while for smaller distances the peak SAR is found near the nose region or the back of the skull (see Fig. 5b). Similar results are obtained with EGT precoding.

C. NORMALIZED EXPOSURE ASSESSMENT

This section presents the normalized exposure β defined in (6). The obtained β-values will be compared with $\beta_{ICNIRP} = 0.05\,m^2/kg$ calculated from the ICNIRP

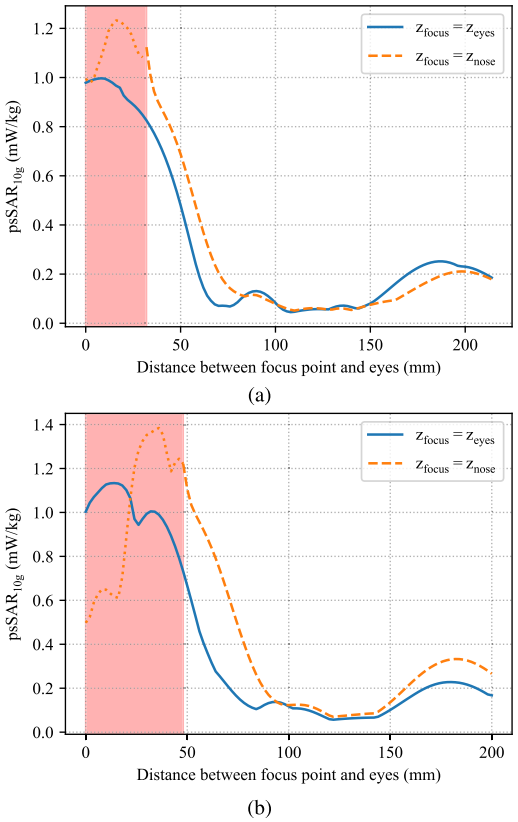


FIGURE 7. **psSAR$_{10g}$ (basic restriction) as a function of the distance between the focus point and the eyes of the (a) Ella and (b) Duke phantoms using MRT precoding. The UE is located in front of the eyes. Two different heights of the focus point are compared, i.e., focus point at the height of the eyes (z_{eyes}) and at the height of the nose (z_{nose}). The red shaded area indicates the border of the eyes and nose. The orange dotted line in the red shaded area shows focus points which are found in the phantom. The precoding weights are normalized according to (2).**

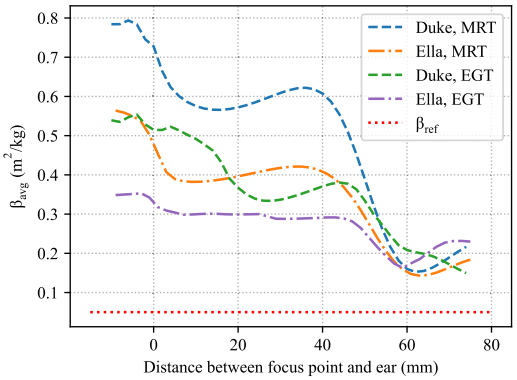


FIGURE 8. **psSAR$_{10g}$ (basic restriction) normalized to the average incident power density (reference level) over the computational domain, i.e., 560 mm × 300 mm × 250 mm (β_{avg}) as a function of distance. The UE is located next to the ear. The red dotted line ($\beta = 0.05\,\mathrm{m^2/kg}$) indicates the reference value obtained with the ICNIRP guidelines for the general public.**

guidelines for the general public, i.e., $\mathrm{SAR}_{10g}^{\mathrm{ICNIRP}} = 2\,\mathrm{W/kg}$, $\mathrm{S}_{\mathrm{inc}}^{\mathrm{ICNIRP}} = 40\,\mathrm{W/m^2}$.

1) FOCUSING AT THE EAR

For this configuration, three different normalizations are compared. In the first, $\mathrm{S_{inc}}(\mathbf{r})$ is averaged over the whole computational domain, leading to β_{avg}. This type of normalization allows us to compare the results for both precoding techniques and phantoms. In the second, $\mathrm{S_{inc}}(\mathbf{r})$ is taken at the focus point ($\mathbf{r} = \mathbf{r}_{\mathrm{UE}}$) leading to β_{focus}. The intended focus point is often not the location where the maximum power density is found, as is seen in Fig. 3. Therefore, in the third normalization, the maximum $S_{\mathrm{inc}}(\mathbf{r}) = S_{\mathrm{inc,\,max}}$ in the domain is taken, leading to β_{max}, which is the ICNIRP approach.

Fig. 8 shows β_{avg} as a function of the distance between the focus point and the ear for both phantoms and both precoding techniques. For all distances, this type of normalization results in exceeding the guidelines ($\beta_{avg} > \beta_{ref}$). Additionally, for larger distances, there is less dependency on the phantom and precoding technique that is used. The curves almost coincide. For smaller distances, there is still a difference in order of magnitude between the two precoding techniques. Looking at Fig. 6, this difference in order of magnitude is smaller than for the non-normalized psSAR$_{10g}$. This means that on average, the power density when using EGT precoding is lower than when using MRT. This can be explained by the higher fields that are found using MRT, which was also seen in Fig. 4. This is expected as MRT uses 2 degrees (amplitude and phase) of freedom versus one (phase) in EGT.

Fig. 9 shows β_{focus} and β_{max} as a function of distance between the focus point and the ear for both phantoms and both precoding techniques. Normalizing to the maximum incident power density (β_{max}) always complies with the guidelines for all distances, that is, $\beta_{max} < \beta_{ref}$. This is also the definition given in the guidelines. However, normalizing to the power density at the focus point, sometimes result in exceeding the limits. In the case of MRT, this only occurs for the smallest distances, while in the case of EGT, this also occurs for distances between 30 and 40 mm. The highest normalized psSAR$_{10g}$ is found when normalizing to $\mathrm{S_{inc,\,focus}}$ for distances < 0 mm. At these distances, a high power density is found near the ear which leads to a high psSAR$_{10g}$, but the power density at the intended focus point is low, leading to a fast decreasing β_{focus} for small distances. In comparison, β_{max} stays relatively constant for all distances. This effect was also seen by the authors of [12]. For larger distances, the two normalizations become similar. This has two reasons. The first is that at these distances, the phantom will not influence the power density at the focus point any more. Note that only $\mathrm{S_{inc,\,max}}$ was taken in free space, i.e., without the phantom present and $\mathrm{S_{inc,\,focus}}$ was determined with the phantom present. The second is that the intended focus point will become the actual focus point, i.e., $\mathrm{S_{inc,\,max}}$ will be found close to the focus point. Additionally, it can be seen that with these normalizations, the order of magnitude of β is the same for both EGT and MRT precoding.

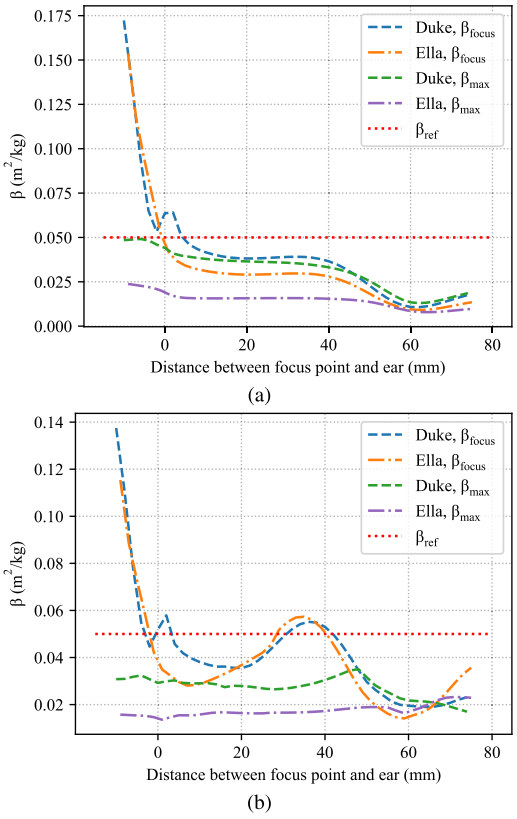


FIGURE 9. $\mathrm{psSAR_{10g}}$ (basic restriction) normalized to $\mathrm{S_{inc,\,focus}}$ and $\mathrm{S_{inc,\,max}}$ (reference level) leading to β_{focus} and β_{max}, respectively, as a function of the distance for (a) MRT. (b) EGT. The UE is located next to the ear. The red dotted line ($\beta = 0.05\,\mathrm{m^2/kg}$) indicates the reference value obtained with the ICNIRP guidelines for the general public.

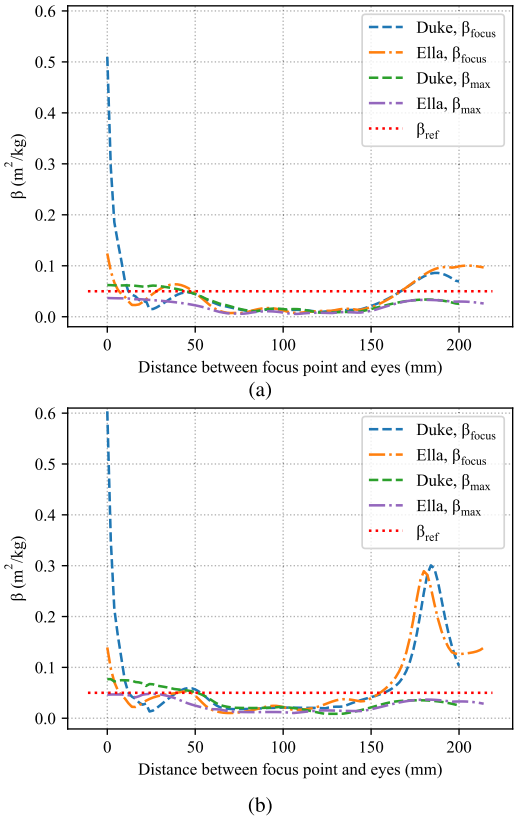


FIGURE 10. $\mathrm{psSAR_{10g}}$ (basic restriction) normalized to $\mathrm{S_{inc,\,focus}}$ and $\mathrm{S_{inc,\,max}}$ (reference level) leading to β_{focus} and β_{max}, respectively, as a function of the distance for (a) MRT. (b) EGT. The UE is located in front of the eyes. The red dotted line ($\beta = 0.05\,\mathrm{m^2/kg}$) indicates the reference value obtained with the ICNIRP guidelines for the general public.

2) FOCUSING AT THE EYES

For this configuration, the same types of normalizations as before are considered with one additional normalization, i.e., normalizing to $\mathrm{S_{inc,V_{avg}}}$, i.e., the power density averaged over a certain volume ($\mathrm{V_{avg}}$) centered around the focus point (UE location).

Fig. 10 plots β_{focus} and β_{max} as a function of distance between the focus point and the eyes for both phantoms and both precoding techniques. Again, it can be seen that the highest values are found when normalizing to $\mathrm{S_{inc,focus}}$ for the smallest distances. Then β_{focus} starts decreasing until it starts increasing again with a peak around 180 mm for both the Duke and Ella phantoms, exceeding the guidelines. This peak is higher using EGT than MRT. In Fig. 7, it was seen that $\mathrm{psSAR_{10g}}$ increases for these distances since high fields occur at the ear. This together with Fig. 10 shows that the power density at the focus ($\mathrm{S_{inc,focus}}$) is lower at these distances using EGT than MRT. The combination of a high $\mathrm{psSAR_{10g}}$ and a low $\mathrm{S_{inc,focus}}$ leads to a peak in β_{focus}. When normalizing to the maximum incident power density, the guidelines are only exceeded for the Duke phantom at the smallest distances up to 50 mm. For distances between 50 and 150 mm, β_{focus} and β_{max} are approximately the same. For these distances, the maximum power density will coincide with the focus point or similar values will be found at the focus point as the maximum.

Fig. 11 shows $\beta_{V_{avg}}$ as a function of distance between the focus point and the eyes for both phantoms using MRT precoding. The averaging volume ($\mathrm{V_{avg}}$) over which $\mathrm{S_{inc}}$ is averaged is varied from $0\,\mathrm{cm^3}$ (focus point) to $10\,\mathrm{cm} \times 10\,\mathrm{cm} \times 10\,\mathrm{cm} = 1000\,\mathrm{cm^3}$. This volume is centered around the focus point which is the reason why not all curves have the same length, i.e., $\mathrm{V_{avg}}$ needs to lie in the computational domain. Additionally, the power density is averaged over the whole domain ($\mathrm{S_{inc,avg}}$). All the curves follow the same behavior as a function of distance. All averaging volumes lead to exceeding the guidelines for certain distances. When $V_{avg} = 8\,\mathrm{cm^3}$ (corresponding with 10g-cube if $\rho = 1000\,\mathrm{kg/m^3}$), $\beta_{V_{avg}}$ complies with the guidelines for almost all distances and only slightly exceeds the limit for the other distances. Fig. 11 demonstrates that $\mathrm{V_{avg}}$ determines whether the basic restrictions are exceeded or not for certain focusing distances while adhering to the reference levels.

In conclusion, the choice of normalization strategy will decide if the guidelines are exceeded or not. We suggested some alternative normalization strategies than the one proposed by ICNIRP, i.e., normalizing to the maximum incident power density. We suggested these because this type

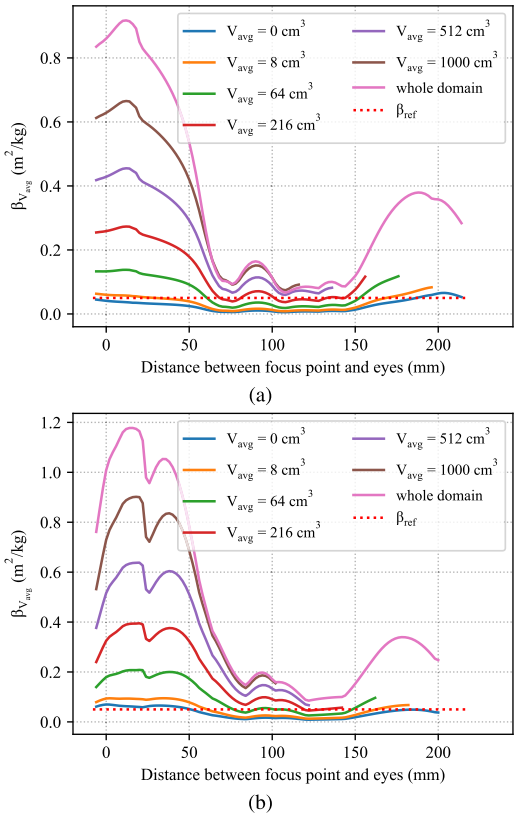


FIGURE 11. **psSAR$_{10g}$ (basic restriction) normalized to $S_{inc,\,V_{avg}}$ (reference level) leading to $\beta_{V_{avg}}$ as a function of distance for the (a) Ella and (b) Duke phantoms using MRT. The UE is located in front of the eyes. The red dotted line ($\beta = 0.05\,\mathrm{m^2/kg}$) indicates the reference value obtained with the ICNIRP guidelines for the general public.**

of exposure is focused around the UE, but that the maximum incident power density is not always found at this point.

D. COMPARISON AND LIMITATIONS

Fig. 4 shows that a focusing of the EMFs at the UE can be achieved by applying MRT and EGT using 80 plane waves. A limitation here is that we make abstraction of the environment and that we assume that the incident EMFs can come from any direction, which is an ideal case. However, Fig. 5 shows that, using these assumptions, an RF-EMF hotspot can be formed at the UE with a hotspot size between 44 and 58 mm, which corresponds with 0.51λ and 0.68λ. This is in line with [10], where a hotspot size of 51 mm $= 0.6\lambda$ is found using numerical simulations. In [10], ray-tracing was used to model the environment. Measurements done at the same frequency also show that the hotspot size is realistic. Our simulation approach was verified in a prior work [22] by comparing the simulated hotspot size induced by MRT with measurements at 3.5 GHz, where a hotspot size of 60 mm $= 0.7\lambda$ was found. Fig. 5 also shows that the exposure will be much more localized than for far-field exposure using a single plane wave [2].

Fig. 6 and 7 demonstrate that the a-DL exposure highly depends on the UE location. Generally, the psSAR$_{10g}$ decreases with increasing distance between the phantom and the UE location. This is similar to the psSAR$_{10g}$ in near-field exposure scenarios, which in general decreases with increasing distance between the antenna and the phantom.

Fig. 8 to 11 show the normalized exposure when normalizing to the incident power density using different definitions. Normalizing using the definition of the ICNIRP guidelines, the limit is only exceeded for the case using the Duke phantom and focusing in front of the eyes at close distance. As already mentioned, the a-DL exposure is highly localized compared to single plane wave exposure. Therefore, it is difficult to compare the obtained exposure values with previous studies, since the literature about single plane wave exposure often only reports the whole-body SAR and not the localized SAR. Another problem is that in the case of single plane wave exposure, the definition of the incident power density is unambiguously, while this is not the case with the focused exposure. In [2], the psSAR$_{10g}$ is investigated for various incident single plane waves. A psSAR$_{10g}$ between 500 and 1200 mW/kg is found for an incident power density of 10 W/m^2. Comparing these values to this study, when using the maximum incident power density (ICNIRP guidelines), slightly lower values are obtained. In this study, values between 60 and 770 mW/kg are found. These values are obtained by multiplying β_{max} by 10 W/m^2. A limitation of this work is that we make an abstraction of the UE device. We only look at the location where the UE would be found, but do not actually model it. In reality, the UE will induce near field coupling with the body, since the user will be situated in the near field of the UE. The user's head will cause shadowing of the UE and the radiation pattern of the UE's antenna will be affected. As a result, not all incident EMFs will contribute equally in the precoding. The authors of [11] investigate this effect. There, a psSAR$_{10g}$ of about 600 mW/kg (for an incident power density of 10 W/m^2) is found when applying MRT and focusing next to the ear of the Duke phantom, which is a similar value as the ones found in this study.

IV. CONCLUSION

A numerical approach is presented to quantify a-DL exposure at 3.5 GHz in terms of localized absorption. Two different precoding techniques were applied to ensure focusing at the UE, which was located near the head to emulate a phone call or video call. More plane waves, representing more available channels for DL, lead to a stronger focusing of the RF-EMFs. The enhancement of the power density at the UE was 7 dB when using EGT and 18 dB when using MRT precoding for 80 incident plane waves. The localized exposure was quantified in terms of the psSAR$_{10g}$ using a female and a male phantom. No significant differences in exposure were found. The distance between the UE and the head was varied to see how this affected the exposure. The peak locations depended on the distance and were found in/near the ear, nose, or the back of the skull. Finally, different normalization

strategies were presented to compare the exposure to the international guidelines. The choice of normalization strategy determines if the ICNIRP basic restriction is exceeded or not while complying with the reference levels. This work was performed at 3.5 GHz, but can easily be extended to higher frequencies. Future work consists of applying this approach at the mm-waves. This will require alternative phantoms due to the high computational cost at these frequencies.

REFERENCES

[1] International Commission on Non-Ionizing Radiation Protection, "Guidelines for limiting exposure to electromagnetic fields (100 kHz to 300 GHz)," *Health Phys.*, vol. 118, no. 5, pp. 483–524, 2020.
[2] T. Uusitupa, I. Laakso, S. Ilvonen, and K. Nikoskinen, "SAR variation study from 300 to 5000 MHz for 15 voxel models including different postures," *Phys. Med. Biol.*, vol. 55, no. 4, pp. 1157–1176, Feb. 2010.
[3] T. L. Marzetta, "Noncooperative cellular wireless with unlimited numbers of base station antennas," *IEEE Trans. Wireless Commun.*, vol. 9, no. 11, pp. 3590–3600, Nov. 2010.
[4] I. Liorni, M. Capstick, L. van Wel, J. Wiart, W. Joseph, E. Cardis, M. Guxens, R. Vermeulen, and A. Thielens, "Evaluation of specific absorption rate in the far-field, near-to-far field and near-field regions for integrative radiofrequency exposure assessment," *Radiat. Protection Dosimetry*, vol. 190, no. 4, pp. 459–472, Oct. 2020.
[5] M. Velghe, S. Aerts, L. Martens, W. Joseph, and A. Thielens, "Protocol for personal RF-EMF exposure measurement studies in 5th generation telecommunication networks," *Environ. Health*, vol. 20, no. 1, pp. 1–10, Dec. 2021.
[6] B. Thors, A. Furuskär, D. Colombi, and C. Törnevik, "Time-averaged realistic maximum power levels for the assessment of radio frequency exposure for 5G radio base stations using massive MIMO," *IEEE Access*, vol. 5, pp. 19711–19719, 2017.
[7] P. Baracca, A. Weber, T. Wild, and C. Grangeat, "A statistical approach for RF exposure compliance boundary assessment in massive MIMO systems," in *Proc. 22nd Int. ITG Workshop Smart Antennas*, Mar. 2018, pp. 1–6.
[8] M. Bonato, L. Dossi, E. Chiaramello, S. Fiocchi, S. Gallucci, G. Tognola, P. Ravazzani, and M. Parazzini, "Human RF-EMF exposure assessment due to access point in incoming 5G indoor scenario," *IEEE J. Electromagn., RF Microw. Med. Biol.*, vol. 5, no. 3, pp. 269–276, Sep. 2021.
[9] Y. Diao and A. Hirata, "Exposure assessment of array antennas at 28 GHz using hybrid spherical near-field transformation and FDTD method," *IEEE Trans. Electromagn. Compat.*, vol. 63, no. 5, pp. 1690–1698, Oct. 2021.
[10] S. Shikhantsov, A. Thielens, G. Vermeeren, E. Tanghe, P. Demeester, L. Martens, G. Torfs, and W. Joseph, "Hybrid ray-tracing/FDTD method for human exposure evaluation of a massive MIMO technology in an industrial indoor environment," *IEEE Access*, vol. 7, pp. 21020–21031, 2019.
[11] S. Shikhantsov, A. Thielens, G. Vermeeren, P. Demeester, L. Martens, G. Torfs, and W. Joseph, "Massive MIMO propagation modeling with user-induced coupling effects using ray-tracing and FDTD," *IEEE J. Sel. Areas Commun.*, vol. 38, no. 9, pp. 1955–1963, Sep. 2020.
[12] S. Shikhantsov, A. Thielens, G. Vermeeren, P. Demeester, L. Martens, and W. Joseph, "Numerical assessment of human EMF exposure to collocated and distributed massive MIMO deployments in an industrial indoor environment," *IEEE Trans. Electromagn. Compat.*, vol. 65, no. 4, pp. 960–971, Aug. 2023.
[13] S. de Miguel-Bilbao, V. Ramos, and J. Blas, "Assessment of polarization dependence of body shadow effect on dosimetry measurements in 2.4 GHz band," *Bioelectromagnetics*, vol. 38, no. 4, pp. 315–321, May 2017.
[14] S. De Miguel-Bilbao, J. Blas, and V. Ramos, "Effective analysis of human exposure conditions with body-worn dosimeters in the 2.4 GHz band," *J. Visualized Exp.*, vol. 135, no. 135, 2018, Art. no. e56525, doi: 10.3791/56525.
[15] H. Herssens and A. Thielens, "Auto-induced, radiofrequency, downlink exposure focused at the human ear," in *Proc. 53rd Eur. Microw. Conf. (EuMC)*, Sep. 2023, pp. 444–447.
[16] C. A. Balanis, *Antenna Theory: Analysis and Design*. Hoboken, NJ, USA: Wiley, 2015.
[17] M.-C. Gosselin, E. Neufeld, H. Moser, E. Huber, S. Farcito, L. Gerber, M. Jedensjö, I. Hilber, F. D. Gennaro, B. Lloyd, E. Cherubini, D. Szczerba, W. Kainz, and N. Kuster, "Development of a new generation of high-resolution anatomical models for medical device evaluation: The virtual population 3.0," *Phys. Med. Biol.*, vol. 59, no. 18, pp. 5287–5303, Sep. 2014.
[18] P. Hasgall, F. Di Gennaro, C. Baumgartner, E. Neufeld, B. Lloyd, M. Gosselin, D. Payne, A. Klingenböck, and N. Kuster, "IT'IS database for thermal and electromagnetic parameters of biological tissues, version 4.0," Found. Res. Inf. Technol. Soc. (IT'IS), Zurich, Switzerland, Feb. 2022, doi: 10.13099/VIP21000-04-1. [Online]. Available: https://itis.swiss/virtual-population/tissue-properties/database/dielectric-properties
[19] S. Saunders and A. Aragón-Zavala, *Antennas and Propagation for Wireless Communication Systems*. Hoboken, NJ, USA: Wiley, 2007.
[20] T. L. Marzetta, E. G. Larsson, H. Yang, and H. Q. Ngo, *Fundamentals of Massive MIMO*. Cambridge, U.K.: Cambridge Univ. Press, 2016.
[21] *IEEE Standard for Safety Levels With Respect to Human Exposure to Electric, Magnetic, and Electromagnetic Fields, 0 Hz to 300 GHz*, Standard Std C95.1-2019 (Revision of IEEE Std C95.1-2005/Incorporates IEEE Std C95.1-2019/Cor 1-2019), 2019, pp. 1–312.
[22] M. Velghe, S. Shikhantsov, E. Tanghe, L. Martens, W. Joseph, and A. Thielens, "Field enhancement and size of radio-frequency hotspots induced by maximum ratio field combining in fifth generation network," *Radiat. Protection Dosimetry*, vol. 190, no. 4, pp. 400–411, Oct. 2020, doi: 10.1093/rpd/ncaa118.



HANNE HERSSENS received the M.Sc. degree in engineering physics from Ghent University, Ghent, Belgium, in 2021, where she is currently pursuing the Ph.D. degree in engineering physics with the Waves Research Group, Department of Information Technology. Her research interests include electromagnetic exposure of humans, on-body antennas, and body-centric wireless communication.



ARNO THIELENS (Senior Member, IEEE) received the M.Sc. and Ph.D. degrees in engineering physics from Ghent University, Ghent, Belgium, in 2010 and 2015, respectively. He was a Postdoctoral Fellow with Ghent University and imec, from 2015 to 2017. From 2017 to 2019, he was a Postdoctoral Fellow with Berkeley Wireless Research Center, University of California at Berkeley, Berkeley, CA, USA. In 2018, he was appointed as a part-time Professor with Ghent University. Simultaneously, he was a Senior Postdoctoral Fellow of the Research Foundation—Flanders (FWO), Brussels, Belgium, from 2020 to 2023. Since 2023, he has been an Associate Professor and the Director of the RF and mm-wave Facility of the Advanced Science and Research Center, Graduate Center of the City University of New York, NY, USA. His main research interests include exposure of living organisms to electromagnetic fields and wireless propagation in and around the human body.